MONTANA STATE UNIVERSITY LIBRARY

Metabolic Responses Induced by Compression of Chondrocytes in Variable-Stiffness Microenvironments

Authors: Carley N. McCutchen, Donald L. Zignego

NOTICE: this is the author's version of a work that was accepted for publication in Journal of Biomechanics. Changes resulting from the publishing process, such as peer review, editing, corrections, structural formatting, and other quality control mechanisms may not be reflected in this document. Changes may have been made to this work since it was submitted for publication. A definitive version was subsequently published in Journal of Biomechanics, VOL# 64, (November 2017) DOI# 10.1016/j.jbiomech.2017.08.032

McCutchen, Carley N. , Donald L. Zignego, and Ronald K. June. "Metabolic Responses Induced by Compression of Chondrocytes in Variable-Stiffness Microenvironments." Journal of Biomechanics (September 2017). DOI: 10.1016/j.jbiomech.2017.08.032.

Made available through Montana State University's ScholarWorks
scholarworks.montana.edu

Metabolic Responses Induced by Compression of Chondrocytes in Variable-Stiffness Microenvironments

Carley N. McCutchen*

Donald L. Zignego*

Ronald K. June*†‡

*Department of Mechanical & Industrial Engineering, Montana State University

†Department of Cell Biology & Neurosciences, Montana State University

‡Department of Orthopaedics & Sports Medicine, University of Washington

Corresponding Author

Ronald K June II
Assistant Professor, Mechanical and Industrial Engineering
Montana State University
PO Box 173800
Bozeman, MT 59717-3800
rjune@montana.edu
406.994.5941 (tel)
406.994.6292 (fax)

Word count: 2913

Keywords: chondrocyte mechanotransduction, cartilage repair, substrate stiffness, osteoarthritis

Abstract

Cells sense and respond to mechanical loads in a process called mechanotransduction. These processes are disrupted in the chondrocytes of cartilage during joint disease. A key driver of cellular mechanotransduction is the stiffness of the surrounding matrix. Many cells are surrounded by extracellular matrix that allows for tissue mechanical function. Although prior studies demonstrate that extracellular stiffness is important in cell differentiation, morphology and phenotype, it remains largely unknown how a cell's biological response to cyclical loading varies with changes in surrounding substrate stiffness. Understanding these processes is important for understanding cells that are cyclically loaded during daily in vivo activities (e.g. chondrocytes and walking). This study uses high-performance liquid chromatography - mass spectrometry to identify metabolomic changes in primary chondrocytes under cyclical compression for 0-30 minutes in low- and high- stiffness environments. Metabolomic analysis reveals metabolites and pathways that are sensitive to substrate stiffness, duration of cyclical compression, and a combination of both suggesting changes in extracellular stiffness in vivo alter mechanosensitive signaling. Our results further suggest that cyclical loading minimizes matrix deterioration and increases matrix production in chondrocytes. This study shows the importance of modeling in vivo stiffness with in vitro models to understand cellular mechanotransduction.

Introduction

Mechanotransduction involves the processes by which cells respond to various forms of mechanical loading such as tension, compression, shear, or hydrostatic pressure. Mechanosensitive pathways are vital for many cellular processes such as metabolism, differentiation, matrix remodeling, and cell survival (Jaalouk and Lammerding, 2009). Cells of structural tissues such as cartilage reside in a dense extracellular matrix that protects the sparse cell population and provides mechanical properties for tissue function. In most tissues, the cells themselves have lower stiffness than their surrounding matrices. Thus, force transmission to the embedded cells is a function of both cell and matrix stiffness (Gao et al., 2014).

Stiffness is a material's resistance to deformation and directly impacts load distribution. Therefore, in two adjacent materials, the one with the lower stiffness will deform more. This explains why cells encapsulated in higher stiffness hydrogels experience larger deformations (Zignego et al., 2014). Cellular force transmission induces conformational changes in the internal structure of the cell, leading to molecular changes that can protect the cells during the dynamic change in environmental conditions (Dowling et al., 2013). Chondrocytes, the lone cell type in cartilage, have an additional matrix called the pericellular matrix (PCM) that forms a thin layer (2-5μm) directly surrounding the cell followed by a common ECM found in other tissues (Youn et al., 2006).

Although past work has recognized the importance of cell and surrounding matrix stiffness on cell differentiation, morphology, and phenotype (Engler et al., 2006; Gilbert et al., 2010; Jianping et al., 2010; Zhang et al., 2016), little is known about the metabolomic response to changes in substrate stiffness. In diseases such as osteoarthritis (OA) there is a direct correlation between disease progression and decreases in stiffness of the PCM directly surrounding the chondrocyte (Zhang, 2015). While healthy cartilage has PCM stiffness values of ~40kPa, the stiffness of osteoarthritic PCM is ~24kPa (Alexopoulos et al., 2005). Current studies have analyzed 3D cultures in 1-3% (v/v) agarose hydrogels, which has a stiffness ranging from 15-19kPa (Jutila et al., 2015), falling to the lower boundary for OA PCM environments and providing limited data on the progression of chondrocyte mechanotransduction pathways from healthy to OA. However, recent advances have characterized mechanical properties of higher concentration agarose hydrogels and found that the stiffness of 4.5% (v/v) agarose hydrogels approaches that of healthy PCM. Therefore,

comparing 2 and 4.5% agarose hydrogels provide an opportunity for studying altered mechanotransduction in OA disease progression (Jutila et al., 2015).

A PCM stiffness value of 35 kPa represents a region between healthy and OA conditions and could potentially give insight on mechanosensitive changes in the cell at early stages of OA before complete cartilage degradation has occurred. Early detection methods for OA patients are currently limited to MRI joint space reduction and family history (Sinusas, 2012). However, if patients and physicians were able to detect cartilage loss prior to stage IV OA, there could be use of therapeutics through physical therapy sessions. Here we analyze the metabolomic profiles of human OA patient chondrocytes after 0- 30 minutes of compression. We find large-scale mechanosensitive changes induced by compression that suggest physical therapy may be a viable option for postponing disease progression or even reversing effects of cartilage matrix deterioration.

The objective of this study is to characterize global differences in cellular behavior at early time points after loading by comparing the metabolomic profiles of cell-encapsulated hydrogels of varying stiffness. In this study, we applied physiological cyclic compression (1.1Hz, 5±1.9% strain) to 2 and 4.5% (v/v) agarose hydrogels containing primary human chondrocytes for 0, 15 and 30 minutes and quantified the changes in metabolism using high-performance liquid chromatography-mass spectrometry (HPLC-MS) and pathway enrichment analysis (Kamburov et al., 2011; Zhu et al., 2013). We hypothesize that cells in higher stiffness hydrogels will show altered mechanosensitive metabolomic profiles compared to cells in lower-stiffness hydrogels due to increased magnitude in transmitted forces to the cells.

Materials and Methods

Primary human chondrocyte culture and encapsulation

As a model of mechanosensitivity in cells undergoing dynamic loading *in vivo*, primary human chondrocytes from grade IV osteoarthritic hips were obtained from n=5 donors following joint replacement. To isolate chondrocytes, harvested cartilage from each patient was digested overnight in Type IV collagenase (2mg/mL for 12-14 h. at 37°C). Isolated chondrocytes were cultured in DMEM with 10% fetal bovine serum and antibiotics (10,000 I.U./mL penicillin and 10,000 μg/mL streptomycin) in 5% CO_2 at 37°C. Cells were expanded in monolayer for one

passage prior to encapsulation in either 2 or 4.5% (v/v) agarose (Sigma: Type VII-A A0701) using previously established methods (Jutila et al., 2014; Zignego et al., 2015). Chondrocytes were seeded at a concentration of ~500,000 cells/gel (gel diameter=7mm, gel height=12.7mm).

Mechanical Stimulation

To model the *in vivo* mechanical environment of chondrocytes, cells were cyclically compressed in 3D agarose hydrogels. Cell-seeded constructs from each patient (N=5 patients, n=3 samples per patient) were randomly assigned to one of three experiment groups: unloaded controls (0 minutes of loading), 15, or 30 minutes of cyclical compression for both 2% and 4.5% experimental groups. 24 hours after encapsulation, the gels were placed in fresh antibiotic-free Dulbecco's Modified Eagle Medium (DMEM) with 10% fetal bovine serum (FBS) and cyclically compressed using a custom built bioreactor (Jutila et al., 2014). This system provides relatively homogeneous deformations with displacement precision of 1% and strain precision of 6.5% (Zignego et al., 2014). Sinusoidal, compressive strains of 5±1.9% (based on initial 12.7mm ± 0.01mm gel height) were applied to the gels at a rate of 1.1 Hz to physiologically mimic the human gait cycle for 0, 15 and 30 minutes (Sutter et al., 2015; Umberger and Martin, 2007). These strains are expected for non-injurious physiological loading. All mechanical testing was performed in physiological cell culture conditions (37°C, 5% CO_2).

Metabolite extraction

To isolate stimulated chondrocytes from agarose hydrogels, cell-seeded constructs were washed twice in phosphate buffered-saline (PBS), immediately flash frozen in liquid nitrogen and pulverized before metabolite extraction in 70:30 methanol:acetone solution. Samples were vortexed every five minutes for the first 20 minutes in solution and held at -20°C overnight for further metabolite extraction. The next day, supernatant was extracted from samples following centrifugation to remove proteins and remaining agarose gel. Metabolite samples were then placed in a centrifuge under vacuum for 6.5 hours for solvent removal. Remaining dried sample pellets were resuspended in 100μL of mass spectrometry grade 95:5 water:acetonitrile solution (Jutila et al., 2014). All reagents were mass-spectrometry grade.

Untargeted metabolic profiling

To identify global changes in cell physiology, we used metabolomic profiling to identify small molecules (metabolites) in control and compressed samples. Extracted metabolites were analyzed using HPLC-MS on an Agilient 6538 quadrupole time-of-flight (QTOF) mass

spectrometer in positive mode (resolution: ~20,000ppm, accuracy: ~5ppm, potential adducts: H^+, Na^+). Intensity values from m/z values identified in each sample were exported using Agilent MassHunter Qualitative Analysis software. Median intensities of m/z values for each experiment group were calculated and statistically analyzed across groups using a student's t test with false-discovery rate correction. M/z values with a q-value < 0.05 between one or more experimental groups were considered statistically significant. Statistically significant m/z values were clustered into co-regulated metabolites using unsupervised clustering in Matlab and extracted for compound identification in METLIN. KEGG and CAS IDs of identified compounds were imported to IMPaLA to assess pathway enrichment with false discovery rate (FDR) analysis ($q < 0.05$) (Kamburov et al., 2011; Zhu et al., 2013).

Results

15 minutes of cyclical compression

Prior studies have examined the long term effects of cyclical loading (***e.g.*** 1-24 hours) but little research has been reported on short term biological implications (Bian et al., 2010; Davisson et al., 2002; Huang et al., 2010; Mauck et al., 2000; Tsuang et al., 2008). Using a 15-minute time scale allows us to identify the transition of a cell's metabolomic profile from a static to dynamic system (Figure 1A). We confirm changes in metabolomic profiles of samples cyclically compressed for 15 minutes compared to unloaded controls as described below.

Clusters A2 and A7 identify metabolites upregulated in either 2 or 4.5%, respectively (Figure 1A). Cluster A2 contains 126 mass-to-charge (m/z) values that map to 8 statistically significant (Student's t-test, $p<0.05$, FDR correction) metabolic pathways including: fatty acid and phospholipid metabolisms, and calcium-dependent pathways. Cluster A7 did not identify any pathways from 108 m/z values.

Clusters A3 to A5 identify metabolites upregulated after 15 minutes of loading: A3-metabolites upregulated in 4.5% agarose only, A4-upregulated in both 2 and 4.5% agarose, and A5-upregulated in only 2% agarose. Enrichment of A3 metabolites resulted in 9 significant pathways including: metabolism of alpha-linolenic acid and retinol, adrenaline signaling, platelet aggregation, vitamin A deficiency, and amino acid degradation. Cluster A4 metabolites represent 2 significant pathways including purine and glutamine/glutamate metabolism for both

2 and 4.5%. Cluster A5 contains 0 significant pathways. Cluster A6 represents metabolites downregulated with 15 minutes of loading and includes 2 statistically significant pathways: butanoate and nicotinamate/nicotinamide metabolism.

30 minutes of cyclical compression

The current treatment option for grade IV OA patients consists of complete joint replacement for patients with excessive pain and discomfort during daily tasks (Sinusas, 2012). The rationale for comparing 0 and 30 minutes of compressive loading is to examine a timescale relevant for treatment options over the duration of a typical physical therapy treatment session. Changes in metabolomic profiles were confirmed for 30-minute loading samples compared to unloaded controls and are detailed below.

Cluster B1 shows a downregulation of metabolite intensity in lysine degradation with 30 minutes of loading (Figure 1B). Clusters B5, B6, B7 and B9 identify metabolites upregulated after 30 minutes of loading: (B5) upregulated in 2% agarose only, (B6) upregulated in both 2 and 4.5% agarose, and (B7) and (B9) both identify metabolites upregulated in 4.5% agarose. Cluster B5 contains 50 statistically significant pathways including fatty acid and phospholipid metabolisms. Cluster B6 identifies 10 significant pathways including alpha-linolenic acid, amino acid, and retinol metabolisms, vitamin A deficiency, and glutathione synthesis and recycling. Cluster B7 did not identify any load-related pathways; however cluster B9 contains 7 significant pathways including fructose, mannose, and alpha-linolenic acid metabolisms as well as chondroitin sulfate and dermatan sulfate degradation.

Cluster B3 does not identify any known pathways upregulated only in 4.5% with or without loading. Cluster B4 identifies an upregulation of acyl chain remodeling of cardiolipin in only 2% agarose with and without loading.

Stiffness-Dependent Mechanotransduction

Comparisons of metabolite distributions for 0, 15, and 30 minute time points between 2% and 4.5% agarose show metabolite values distinct to each stiffness group (Figure 2A) and loading conditions (Supplemental Figure 2). Principal Components Analysis (PCA) analysis revealed distinct clustering of all experimental groups with PCA components 1, 2, and 3 representing 30.0%, 8.9% and 7.1% of the total variance, respectively.

Comparing unloaded 2% cell-encapsulated hydrogels with the other 5 experimental groups revealed over 200 m/z values that were detected in unloaded 2% samples that were not detected in all other samples (Figure 2B). In contrast, over 300 m/z values were not detected in unloaded 2% samples that we detected in all other experiment groups revealing both loading- and stiffness-induced changes in metabolomic profiles.

We found significant changes in the distributions of metabolite intensities only when comparing 0 vs 15 minutes and 0 vs 30 minutes in 4.5% agarose hydrogels, not 2% hydrogels (Figure 3). Comparisons between 2% loading groups reveal no significant changes between 0-, 15- and 30-minute time points suggesting that the higher stiffness associated with 4.5% agarose is required for mechanotransduction. These data may also represent the decreased sensitivity in osteoarthritic chondrocytes to dynamic loading vital for cell survival and extracellular matrix production.

Discussion

After exposing primary human chondrocytes encapsulated in agarose hydrogels to cyclical compression, we observe changes in metabolomic profiles between high– and low-stiffness hydrogels. When comparing 0-, 15- and 30-minute loading groups, data and analyses show that the metabolomic profiles of chondrocytes are substantially altered with as little as 15 minutes of mechanical stimulus (Figure 1A). Using pathway analysis, cellular signaling pathways were uniquely identified varying with time and hydrogel stiffness. The differences in pathway upregulation/downregulation suggest microenvironmental sensitivity to mechanical loading in cell metabolism (Figure 4). Based on prior results, we estimate that the average stresses are at least 40% higher in the 4.5% agarose samples compared with the 2% agarose samples.

<u>Pathways similarly regulated in 2 and 4.5% microenvironments</u>

Upregulated with loading

15 minutes of loading in both 2 and 4.5% agarose hydrogels upregulated purine, glutamine and glutamate metabolism pathways. The result of increased purine metabolism may correspond to known adenosine signaling regulating bone and cartilage health (Strazzulla and Cronstein, 2016). The intracellular and extracellular production of adenosine, a purine

nucleoside, acts in response to mechanical stimulation including inflammation. This interaction occurs at the P2-A2A receptor, which has been shown to regulate chondrocyte differentiation and function (Campo et al., 2012). Without tight regulation of extracellular adenosine levels, increases in glycosaminoglycan (GAG) release, matrix metalloproteinase production, prostaglandin E2 and nitric oxide (NO) can induce further inflammation and potentially lead to cell death. Upregulation of glutamine and glutamate metabolism may indicate tricarboxylic acid (TCA) cycle compound alpha-ketoglutarate is being converted to glutamate/glutamine to produce additional building blocks for protein synthesis of matrix molecules. Increased levels of glutamine might also be a cellular survival response to increased nitric oxide production during excess articular chondrocyte activation with loading (Studer et al., 1999). Excess glutamine has been shown to inhibit NO-induced apoptosis in articular chondrocytes (Tonomura et al., 2006).

30 minutes of loading in both 2% and 4.5% agarose upregulated the same pathways as 15 minutes of loading in only 4.5% agarose gels. This suggests a latent mechanosensitive response in low-stiffness microenvironments compared to high-stiffness conditions. These pathways consist of adrenaline signaling, alpha-linolenic acid and retinol metabolism, vitamin A deficiency, and amino acid degradation. Adrenaline signaling through norepinephrine (m/z: 170.0807, adduct: $M+H^+$) previously has been linked to increased apoptosis and the reduction of chondrocyte proliferation in OA cell cultures (Lorenz et al., 2016). Anti-inflammatory and tissue protective effects have been shown in 1:1 to 6:1 ratios of linoleic acid (LA) to alpha-linolenic acid (ALA) inhibiting the decomposition of connective tissue such as type II collagen compared to higher ratios (*e.g.* 10:1) that induce inflammatory responses (Mengshol et al., 2000; Yu et al., 2015). Further targeted analyses would be required to determine the LA to ALA ratio accurately.

Finally, we see the upregulation of glutathione synthesis and recycling in 30 minutes of loading in both 2 and 4.5% hydrogels only (not unloaded controls) further validating our interpretation of oxidative stress minimization (Watari et al., 2011).

Downregulated with loading

Nicotinamate/nicotinamide metabolism, essential for generating coenzymes nicotinamide adenine dinucleotide (NAD+) and nicotinamide adenine dinucleotide phosphate (NADP+), used in glycolysis, TCA cycle, pentose phosphate cycle, fatty acid synthesis and other metabolic pathways, showed a statistically significant decrease in intensity after 15

minutes of loading in both 2 and 4.5% hydrogels. Finally the deactivation of lysine degradation upon 30 minutes of dynamic loading in both 2 and 4.5% hydrogels is consistent with mechanically-induced protein/matrix synthesis.

Taken together, these data identify pathways that are sensitive to mechanical compression but independent of substrate stiffness. They further demonstrate that lower-stiffness gels may correspond to delayed mechanosensitive responses leading to imbalances in catabolic and anabolic regulation in cell health leading to further disease progression.

Pathways uniquely regulated in 2 and 4.5% microenvironments

Metabolites found only in 4.5% agarose hydrogels for 0 and 15 minutes of loading (Figure 1A, A7) and 0 and 30 minutes of loading (Figure 1B, B3) fail to identify any statistically significant pathways suggesting large mechanobiological differences between loaded and unloaded controls in higher stiffness microenvironments. In contrast, we find upregulation of fatty acid and phospholipid metabolism throughout all of 2% agarose conditions (Figure 1A, A2 and Figure 1B, B4 and B5) with as many as 50 pathways upregulated in 30 minutes of loading, consistent with increased sensitivity among cells embedded in a lower stiffness matrix leading to increased cell membrane remodeling.

Interestingly, chondroitin and dermatan sulfate, known GAGs in the extracellular matrix of connective tissues, were upregulated in unloaded controls and 30 minutes of cyclical compression in 4.5% hydrogels but were not detected at the 15-minute time point. 30 minutes of cyclical loading in 4.5% agarose hydrogels only resulted in upregulation of several sugar metabolism pathways, consistent with increased GAG production. These pathways were not identified in 2% hydrogel conditions.

Overall, we demonstrate for the first time large-scale changes in chondrocyte mechanotransduction that are dependent on microenvironmental stiffness using metabolomic profiling. These data suggest a link between cartilage matrix deterioration and altered mechanotransduction in OA that could be reversed through therapeutic loading of cartilage (*e.g.* physical therapy).

Acknowledgements

We thank Drs. Brian Bothner and Jonathan Hilmer (Montana State University) for assistance with mass spectrometry. Funding provided by NSF (1342420 and 1554708) and the Montana University System Research Initiative (51040-MUSRI2015-03).

Conflict of Interest Statement

The authors have no financial interest methods, data, or intepretations presented in this manuscript. Dr. June holds stock in Beartooth Biotech which was not involved in this study.

CAPTIONS

Table 1

The number of m/z values in each cluster found in Figure 1, the number of candidate metabolites identified using Metlin (15ppm accuracy, possible adducts: H+ and Na+) and the number of statistically significant pathways identified in IMPaLA using metabolite KEGG and CAS IDs.

Table 2

Table 2. Pathway analysis associated with 0 vs. 15 minute loading heat map Table lists significant cell metabolism pathways identified in each cluster using IMPaLA enrichment analysis and the metabolites associated with positively identified metabolites in that pathway.

Table 3

Table 3. Pathway analysis associated with 0 vs. 30 minute loading heat map (Figure 1B). Table lists significant cell metabolism pathways identified in each cluster using IMPaLA enrichment analysis and the metabolites associated with positively identified metabolites in that pathway.

Figure 1

Mechanotransduction is regulated by both gel stiffness and mechanical loading.

Groupings of metabolites found in (A) 0 and 15 minute loading samples and (B) 0 and 30 minute loading samples from both low-stiffness (2%) and high-stiffness (4.5%) agarose samples using Matlab's heat map hierarchical clustering on the median values. Clusters of interested are outlined and labeled on the right hand side. Cluster A1: On in 2% 0 minute loading only, A2: On in 2% only, A3: On in 4.5% 15 minute loading only, A4: On with 15 minute loading, A5: On 2% 15 minute loading only, A6: Off with loading, A7: On in 4.5% only, A8: On in 4.5% 0 minute loading only. Cluster B1: Off with loading, B2: On with 4.5% 0 minute loading only, B3: On in 4.5% only, B4: On in 2% only, B5: On in 2% 30 minute loading only, B6: On with loading, B7 and B9: On with 4.5% 30 minute loading only, and B8: On in 2% 0 minute loading only.

Figure 2

Both gel stiffness and compression result in large-scale changes in metabolites (A) Comparison of metabolite intensity values found in 0-, 15- and 30- minute loading in 2 and 4.5% agarose hydrogels: (Left) comparison of 0-minute loading between 2% (x-axis) and 4.5% (y-axis) metabolite intensity values. 391 statistically significant metabolite intensity values were uniquely identified in 4.5% agarose while 361 were uniquely identified in 2%. (Center) Comparing 15-minute loading groups between 2% (x-axis) and 4.5% (y-axis) agarose found 383 metabolites specific to 4.5% agarose compared to 238 specific to 2%. (Right) Comparing 30 minutes of loading between 2% (x-axis) and 4.5% (y-axis) found 422 metabolites specific to 4.5% agarose compared to 262 specific to 2%. (B) Barplots showing the number of metabolites in each experimental group showing statistically significant upregulation, downregulation and no change compared to 0 minutes of loading in 2% agarose with FDR correction. Blue denoting upregulation, red downregulation and grey as no significant change in intensity. (C) Principal component analysis of 0-, 15-, and 30-minute experimental groups in 2 and 4.5% agarose (Yellow triangle: 0-minute loading in 2% agarose, purple triangle: 15-minute loading in 2%, red triangle: 30-minute loading in 2%, green circle: 0-minute loading in 4.5%, cyan circle: 15-minute loading in 4.5% and dark blue circle: 30-minute loading in 4.5%). Comparisons of principal component 1 (x-axis, 30%) and 2 (y-axis, 8.9%) (Top) and principal components 2 (x-axis, 8.9%) and 3 (y-axis, 7.1%) (Bottom) show clustering of experiment groups with significant overlap of 0-minute loading in 2 and 4.5% agarose.

Figure 3

Mechanical loading changes distributions of metabolites in 4.5% but not 2% agarose. KS analysis comparing metabolite distributions between experimental groups reveal statistically significant ($p <= 0.05$) changes in metabolomic profiles between 0 and 15 minutes of loading in 4.5% agarose hydrogels (top right) and 0 and 30 minutes of loading in 4.5% agarose hydrogels (middle right). KS analysis of 2% hydrogels (left column) reveal no statistically significant changes in metabolomic profiles with varying loading conditions. Median distributions between 15 and 30 minutes in 4.5% agarose were not significantly different (bottom right).

Figure 4

Summary of chondrocyte metabolomic pathways sensitive to both substrate stiffness and compressive loading. Metabolomic pathways upregulated and downregulated in 2 and

4.5% agarose comparing (A) 0 vs 15 minutes and (B) 0 vs 30 minutes of compression using Metlin and IMPaLA pathway enrichment results from HPLC-MS analysis. PL: phospholipid.

References

Alexopoulos, L.G., Williams, G.M., Upton, M.L., Setton, L.A., Guilak, F., 2005. Osteoarthritic changes in the biphasic mechanical properties of the chondrocyte pericellular matrix in articular cartilage. Journal of biomechanics 38, 509-517.

Bian, L., Fong, J.V., Lima, E.G., Stoker, A.M., Ateshian, G.A., Cook, J.L., Hung, C.T., 2010. Dynamic mechanical loading enhances functional properties of tissue-engineered cartilage using mature canine chondrocytes. Tissue engineering. Part A 16, 1781-1790.

Campo, G.M., Avenoso, A., D'Ascola, A., Scuruchi, M., Prestipino, V., Nastasi, G., Calatroni, A., Campo, S., 2012. Adenosine A2A receptor activation and hyaluronan fragment inhibition reduce inflammation in mouse articular chondrocytes stimulated with interleukin-1beta. The FEBS journal 279, 2120-2133.

Davisson, T., Kunig, S., Chen, A., Sah, R., Ratcliffe, A., 2002. Static and dynamic compression modulate matrix metabolism in tissue engineered cartilage. Journal of orthopaedic research : official publication of the Orthopaedic Research Society 20, 842-848.

Dowling, E.P., Ronan, W., McGarry, J.P., 2013. Computational investigation of in situ chondrocyte deformation and actin cytoskeleton remodelling under physiological loading. Acta biomaterialia 9, 5943-5955.

Engler, A.J., Sen, S., Sweeney, H.L., Discher, D.E., 2006. Matrix elasticity directs stem cell lineage specification. Cell 126, 677-689.

Gao, Y., Liu, S., Huang, J., Guo, W., Chen, J., Zhang, L., Zhao, B., Peng, J., Wang, A., Wang, Y., Xu, W., Lu, S., Yuan, M., Guo, Q., 2014. The ECM-cell interaction of cartilage extracellular matrix on chondrocytes. BioMed research international 2014, 648459.

Gilbert, P.M., Havenstrite, K.L., Magnusson, K.E., Sacco, A., Leonardi, N.A., Kraft, P., Nguyen, N.K., Thrun, S., Lutolf, M.P., Blau, H.M., 2010. Substrate elasticity regulates skeletal muscle stem cell self-renewal in culture. Science (New York, N.Y.) 329, 1078-1081.

Huang, A.H., Farrell, M.J., Kim, M., Mauck, R.L., 2010. Long-term dynamic loading improves the mechanical properties of chondrogenic mesenchymal stem cell-laden hydrogel. European cells & materials 19, 72-85.

Jaalouk, D.E., Lammerding, J., 2009. Mechanotransduction gone awry. Nature reviews. Molecular cell biology 10, 63-73.

Jianping, F., Yang-Kao, W., Yang, M.T., Desai, R.A., Xiang, Y., Zhijun, L., Chen, C.S., 2010. Mechanical regulation of cell function with geometrically modulated elastomeric substrates. Nature Methods Vol. 7, p733-736.

Jutila, A.A., Zignego, D.L., Hwang, B.K., Hilmer, J.K., Hamerly, T., Minor, C.A., Walk, S.T., June, R.K., 2014. Candidate mediators of chondrocyte mechanotransduction via targeted and untargeted metabolomic measurements. Archives of biochemistry and biophysics 545, 116-123.

Jutila, A.A., Zignego, D.L., Schell, W.J., June, R.K., 2015. Encapsulation of chondrocytes in high-stiffness agarose microenvironments for in vitro modeling of osteoarthritis mechanotransduction. Annals of biomedical engineering 43, 1132-1144.

Kamburov, A., Cavill, R., Ebbels, T.M., Herwig, R., Keun, H.C., 2011. Integrated pathway-level analysis of transcriptomics and metabolomics data with IMPaLA. Bioinformatics (Oxford, England) 27, 2917-2918.

Lorenz, J., Schafer, N., Bauer, R., Jenei-Lanzl, Z., Springorum, R.H., Grassel, S., 2016. Norepinephrine modulates osteoarthritic chondrocyte metabolism and inflammatory responses. Osteoarthritis and cartilage 24, 325-334.

Mauck, R.L., Soltz, M.A., Wang, C.C., Wong, D.D., Chao, P.H., Valhmu, W.B., Hung, C.T., Ateshian, G.A., 2000. Functional tissue engineering of articular cartilage through dynamic loading of chondrocyte-seeded agarose gels. Journal of biomechanical engineering 122, 252-260.

Mengshol, J.A., Vincenti, M.P., Coon, C.I., Barchowsky, A., Brinckerhoff, C.E., 2000. Interleukin-1 induction of collagenase 3 (matrix metalloproteinase 13) gene expression in chondrocytes requires p38, c-Jun N-terminal kinase, and nuclear factor kappaB: differential regulation of collagenase 1 and collagenase 3. Arthritis and rheumatism 43, 801-811.

Sinusas, K., 2012. Osteoarthritis: diagnosis and treatment. American family physician 85, 49-56.

Strazzulla, L.C., Cronstein, B.N., 2016. Regulation of bone and cartilage by adenosine signaling. Purinergic signalling 12, 583-593.

Studer, R., Jaffurs, D., Stefanovic-Racic, M., Robbins, P.D., Evans, C.H., 1999. Nitric oxide in osteoarthritis. Osteoarthritis and cartilage 7, 377-379.

Sutter, E.G., Widmyer, M.R., Utturkar, G.M., Spritzer, C.E., Garrett, W.E., Jr., DeFrate, L.E., 2015. In vivo measurement of localized tibiofemoral cartilage strains in response to dynamic activity. The American journal of sports medicine 43, 370-376.

Tonomura, H., Takahashi, K.A., Mazda, O., Arai, Y., Inoue, A., Terauchi, R., Shin-Ya, M., Kishida, T., Imanishi, J., Kubo, T., 2006. Glutamine protects articular chondrocytes from heat stress and NO-induced apoptosis with HSP70 expression. Osteoarthritis and cartilage 14, 545-553.

Tsuang, Y.H., Lin, Y.S., Chen, L.T., Cheng, C.K., Sun, J.S., 2008. Effect of dynamic compression on in vitro chondrocyte metabolism. The International journal of artificial organs 31, 439-449.

Umberger, B.R., Martin, P.E., 2007. Mechanical power and efficiency of level walking with different stride rates. The Journal of experimental biology 210, 3255-3265.

Watari, T., Naito, K., Sakamoto, K., Kurosawa, H., Nagaoka, I., Kaneko, K., 2011. Evaluation of the effect of oxidative stress on articular cartilage in spontaneously osteoarthritic STR/OrtCrlj mice by measuring the biomarkers for oxidative stress and type II collagen degradation/synthesis. Experimental and therapeutic medicine 2, 245-250.

Youn, I., Choi, J.B., Cao, L., Setton, L.A., Guilak, F., 2006. Zonal variations in the three-dimensional morphology of the chondron measured in situ using confocal microscopy. Osteoarthritis and cartilage 14, 889-897.

Yu, H., Li, Y., Ma, L., Meng, H., Bai, X., Fan, Z., Yu, F., Guo, A., 2015. A low ratio of n-6/n-3 polyunsaturated fatty acids suppresses matrix metalloproteinase 13 expression and reduces adjuvant-induced arthritis in rats. Nutrition research (New York, N.Y.) 35, 1113-1121.

Zhang, Q., Yu, Y., Zhao, H., 2016. The effect of matrix stiffness on biomechanical properties of chondrocytes. Acta biochimica et biophysica Sinica 48, 958-965.

Zhang, Z., 2015. Chondrons and the pericellular matrix of chondrocytes. Tissue engineering. Part B, Reviews 21, 267-277.

Zhu, Z.J., Schultz, A.W., Wang, J., Johnson, C.H., Yannone, S.M., Patti, G.J., Siuzdak, G., 2013. Liquid chromatography quadrupole time-of-flight mass spectrometry characterization of metabolites guided by the METLIN database. Nature protocols 8, 451-460.

Zignego, D.L., Hilmer, J.K., June, R.K., 2015. Mechanotransduction in primary human osteoarthritic chondrocytes is mediated by metabolism of energy, lipids, and amino acids. Journal of biomechanics 48, 4253-4261.

Zignego, D.L., Jutila, A.A., Gelbke, M.K., Gannon, D.M., June, R.K., 2014. The mechanical microenvironment of high concentration agarose for applying deformation to primary chondrocytes. Journal of biomechanics 47, 2143-2148.

Figure 1

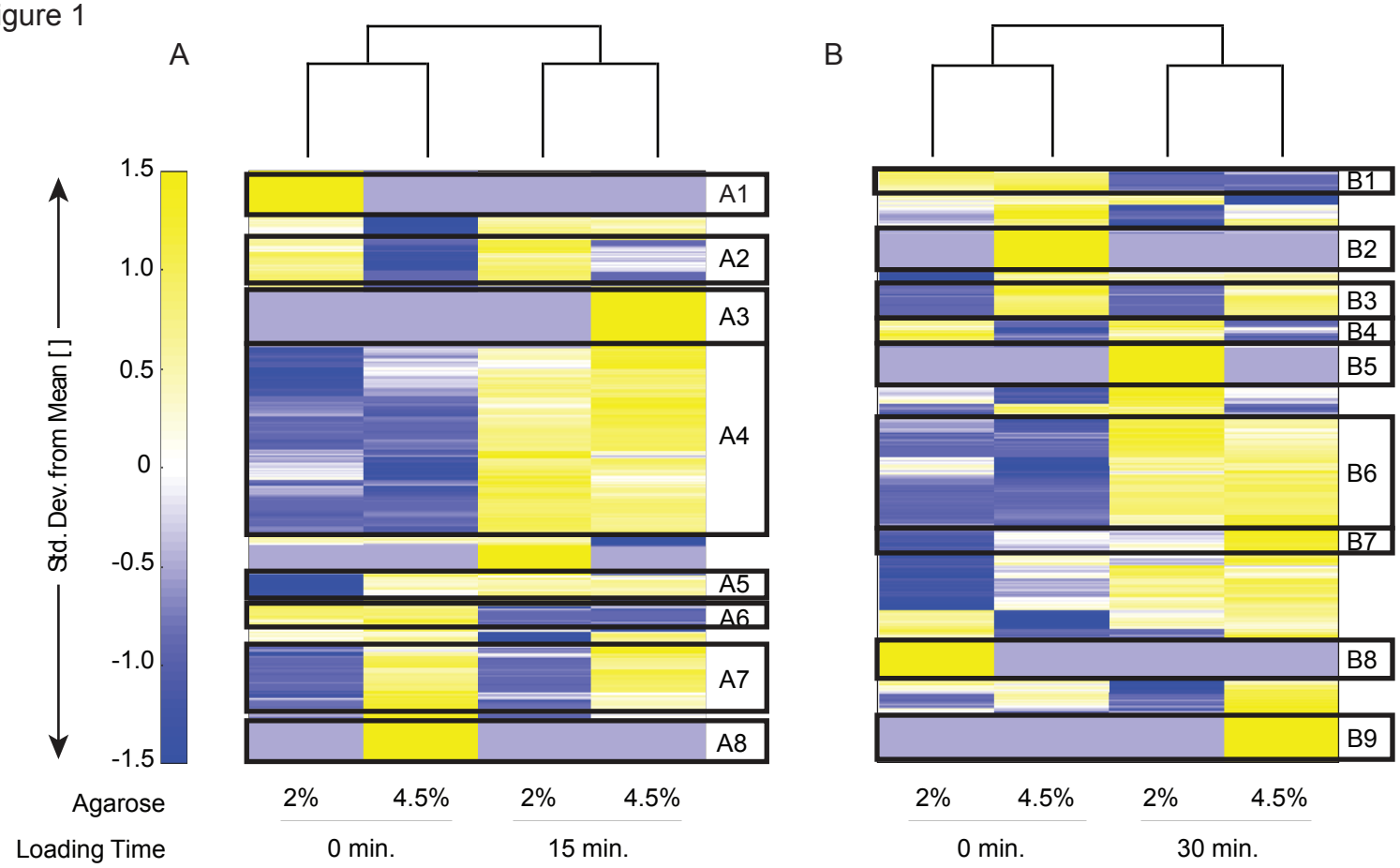
A
B
1.5
1.0
0.5
0
-0.5
-1.0
-1.5
Std. Dev. from Mean [ ]
A1
A2
A3
A4
A5
A6
A7
A8
B1
B2
B3
B4
B5
B6
B7
B8
B9
2%
4.5%
2%
4.5%
Agarose
Loading Time
0 min.
15 min.
2%
4.5%
2%
4.5%
0 min.
30 min.

Figure 2

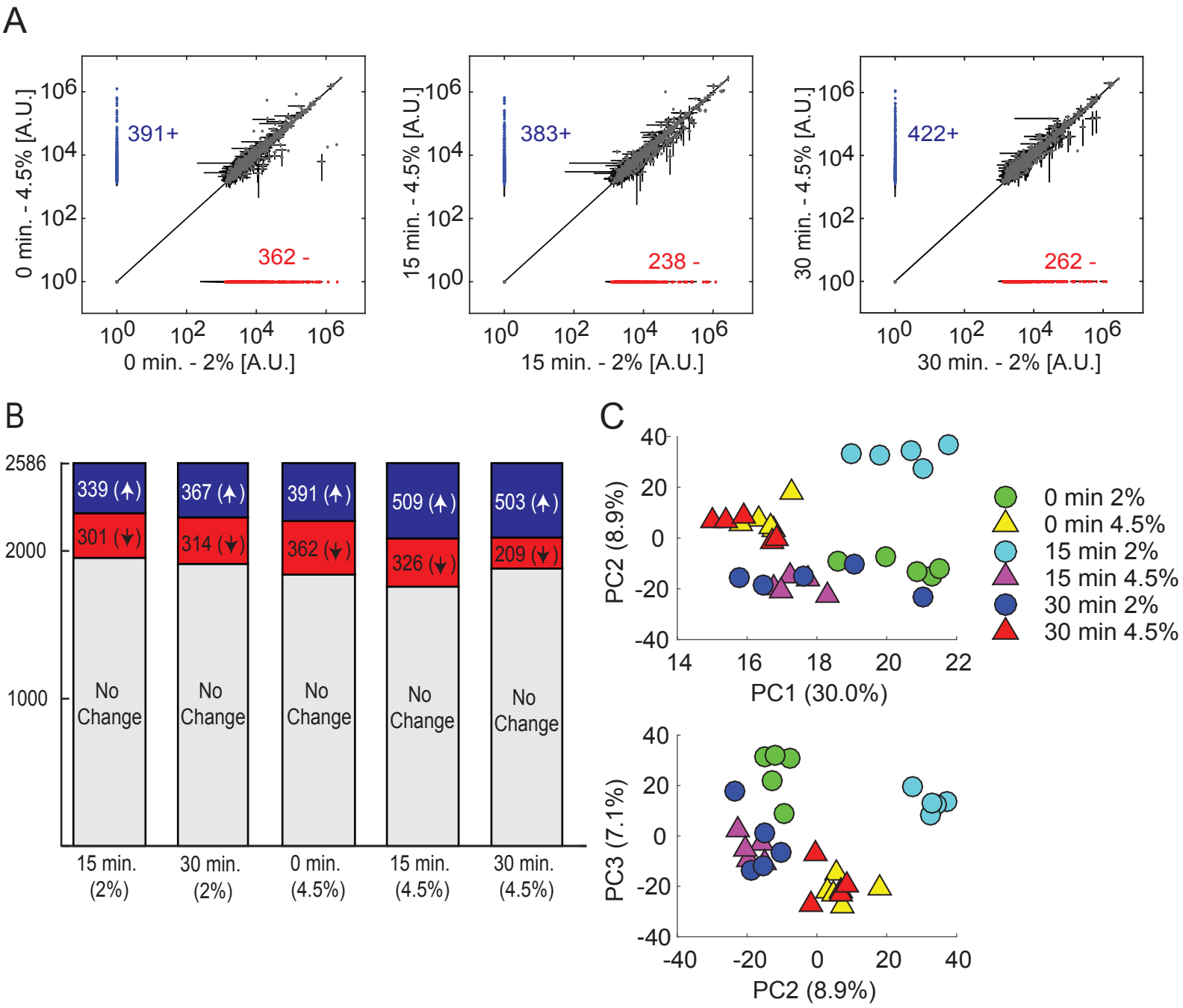
A
391+
362 -
0 min. - 4.5% [A.U.]
0 min. - 2% [A.U.]
383+
238 -
15 min. - 4.5% [A.U.]
15 min. - 2% [A.U.]
422+
262 -
30 min. - 4.5% [A.U.]
30 min. - 2% [A.U.]
B
2586
2000
1000
339 (↑)
301 (↓)
367 (↑)
314 (↓)
391 (↑)
362 (↓)
509 (↑)
326 (↓)
503 (↑)
209 (↓)
No Change
15 min. (2%)
30 min. (2%)
0 min. (4.5%)
15 min. (4.5%)
30 min. (4.5%)
C
PC2 (8.9%)
PC1 (30.0%)
PC3 (7.1%)
PC2 (8.9%)
0 min 2%
0 min 4.5%
15 min 2%
15 min 4.5%
30 min 2%
30 min 4.5%

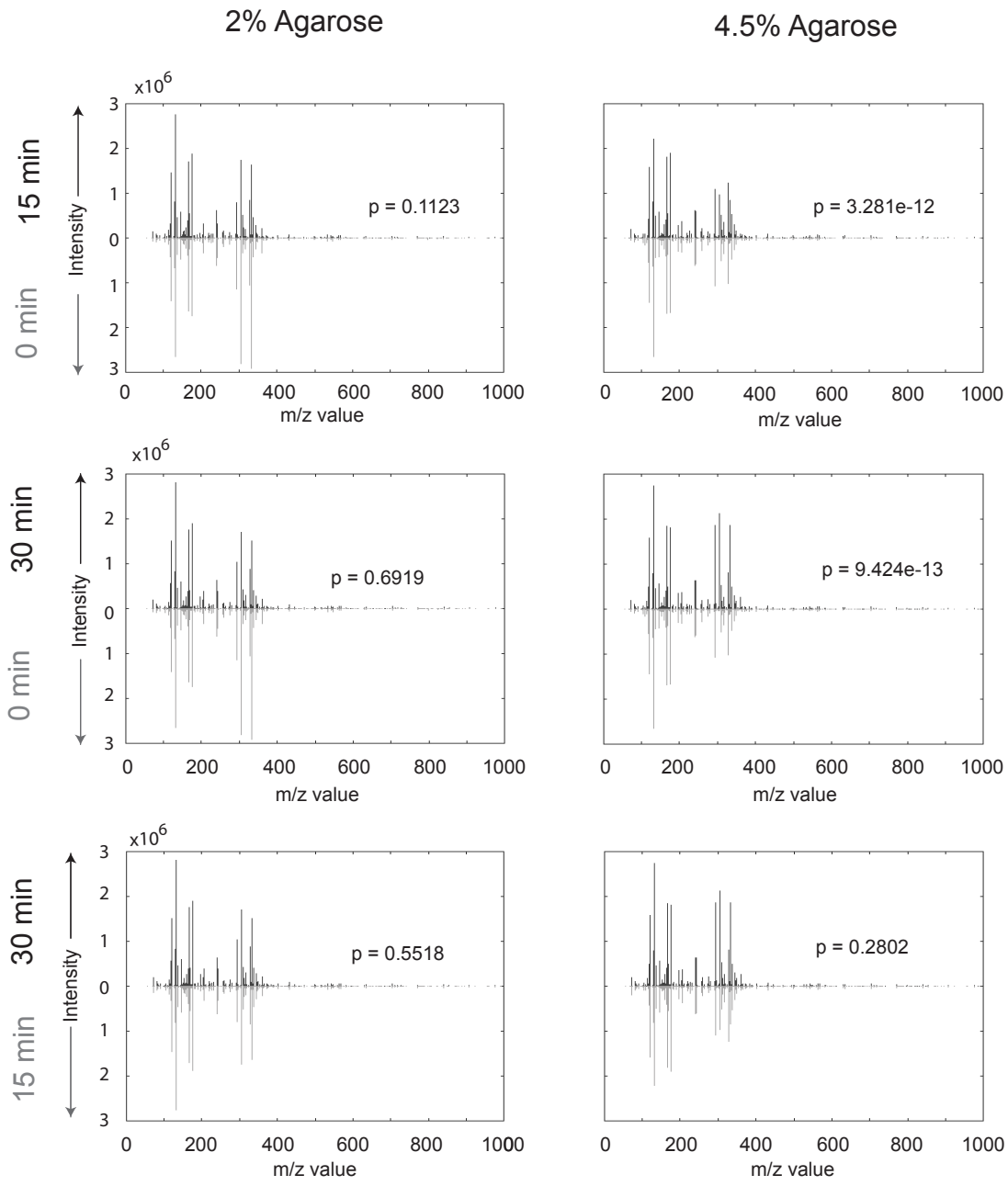
2% Agarose
4.5% Agarose
15 min
0 min
30 min
0 min
30 min
15 min
Intensity
x10^6
m/z value
p = 0.1123
p = 3.281e-12
p = 0.6919
p = 9.424e-13
p = 0.5518
p = 0.2802

A

Compression	Agarose Concentration: 2%		Agarose Concentration: 4.5%	
	UP: Metabolism of Butanoate, Nicotinate & Nicotinamide **DOWN:** Metabolism of D-glutamine/D-glutamate and Purine			
0 min	**UP:** Fatty acid/ PL metabolism (7), Calcium dependent events **DOWN:** N/A	**UP:**Linoleic acid metabolism	**UP:** Degradation of chondroitin and dermatin sulfate, Sugar metabolism (5)	**UP:** N/A **DOWN:** Fatty acid/PL metabolism (7), Calcium dependent events
15 min		**UP:** N/A	**UP:** Metabolism of: Retinol, Alpha-linolenic acid, amino acids. Vitamin A deficiency, Adrenaline signaling (4)	
	UP: Metabolism of D-glutamine/D-glutamate and Purine **DOWN:** Metabolism of Butanoate, Nicotinate & Nicotinamide			

B

Compression	Agarose Concentration: 2%		Agarose Concentration: 4.5%	
	UP: Lysine degradation **DOWN:** Metabolism of: Retinol, Alpha-linolenic acid, amino acids (2), D-glutamine/D-glutamate, and xenobiotics by cytochrome P450. Vitamin C deficiency, Glutathione synthesis and recycling (2)			
0 min	**UP:** Fatty acid/PL metabolism **DOWN:** N/A	**UP:** N/A	**UP:** Degradation of chondroitin and dermatin sulfate, Sugar metabolism (24), Pentose phosphate pathway	**UP:** N/A **DOWN:** Fatty acid/PL metabolism
30 min		**UP:** Fatty acid/PL metabolism	**UP:** Degradation of chondroitin and dermatin sulfate, Alpha-linolenic & Sugar metabolism (3),Aromatase inhibitor pathway	
	UP: Metabolism of: Retinol, Alpha-linolenic acid, amino acids (2), D-glutamine/D-glutamate, and xenobiotics by cytochrome P450. Vitamin C deficiency, Glutathione synthesis and recycling (2) **DOWN:** Lysine degradation			

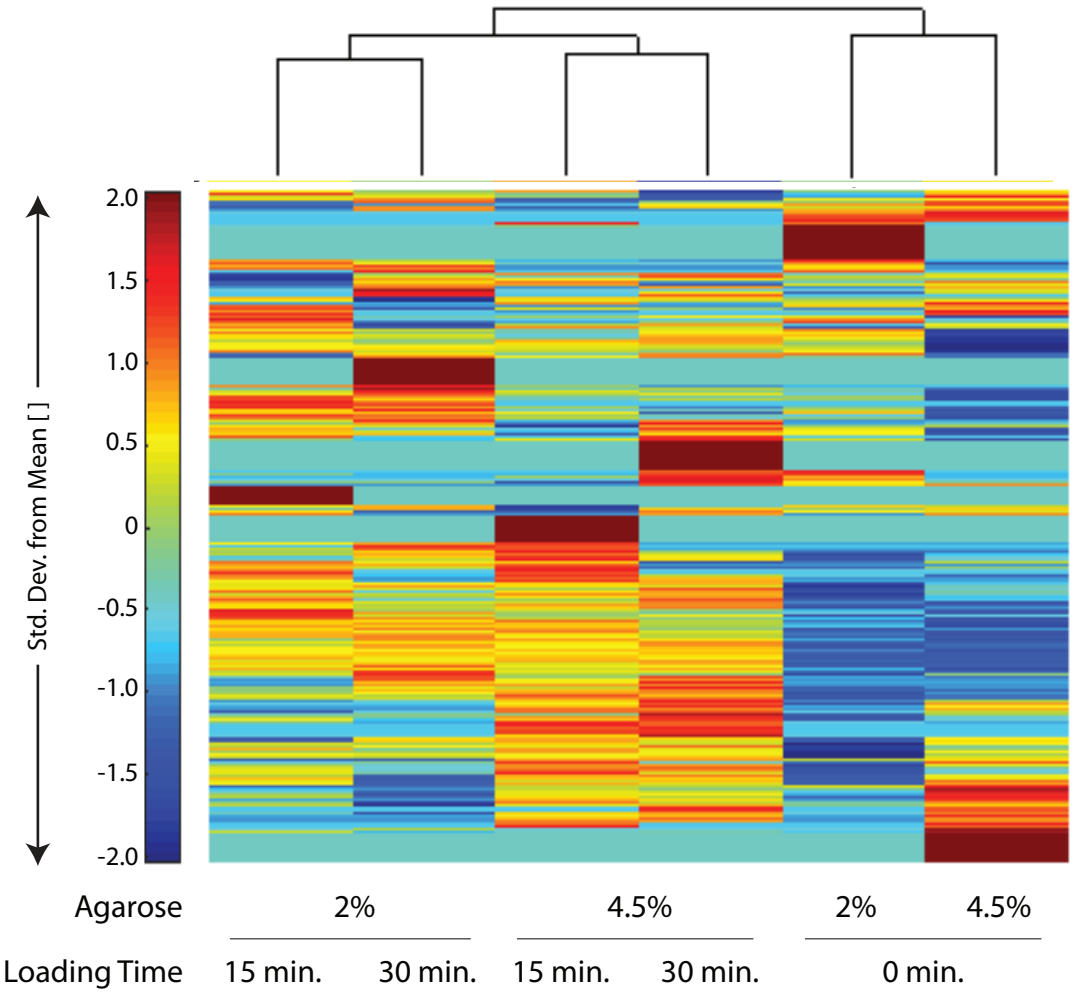
Std. Dev. from Mean [ ]
2.0
1.5
1.0
0.5
0
-0.5
-1.0
-1.5
-2.0
Agarose
2%
4.5%
2%
4.5%
Loading Time
15 min.
30 min.
15 min.
30 min.
0 min.

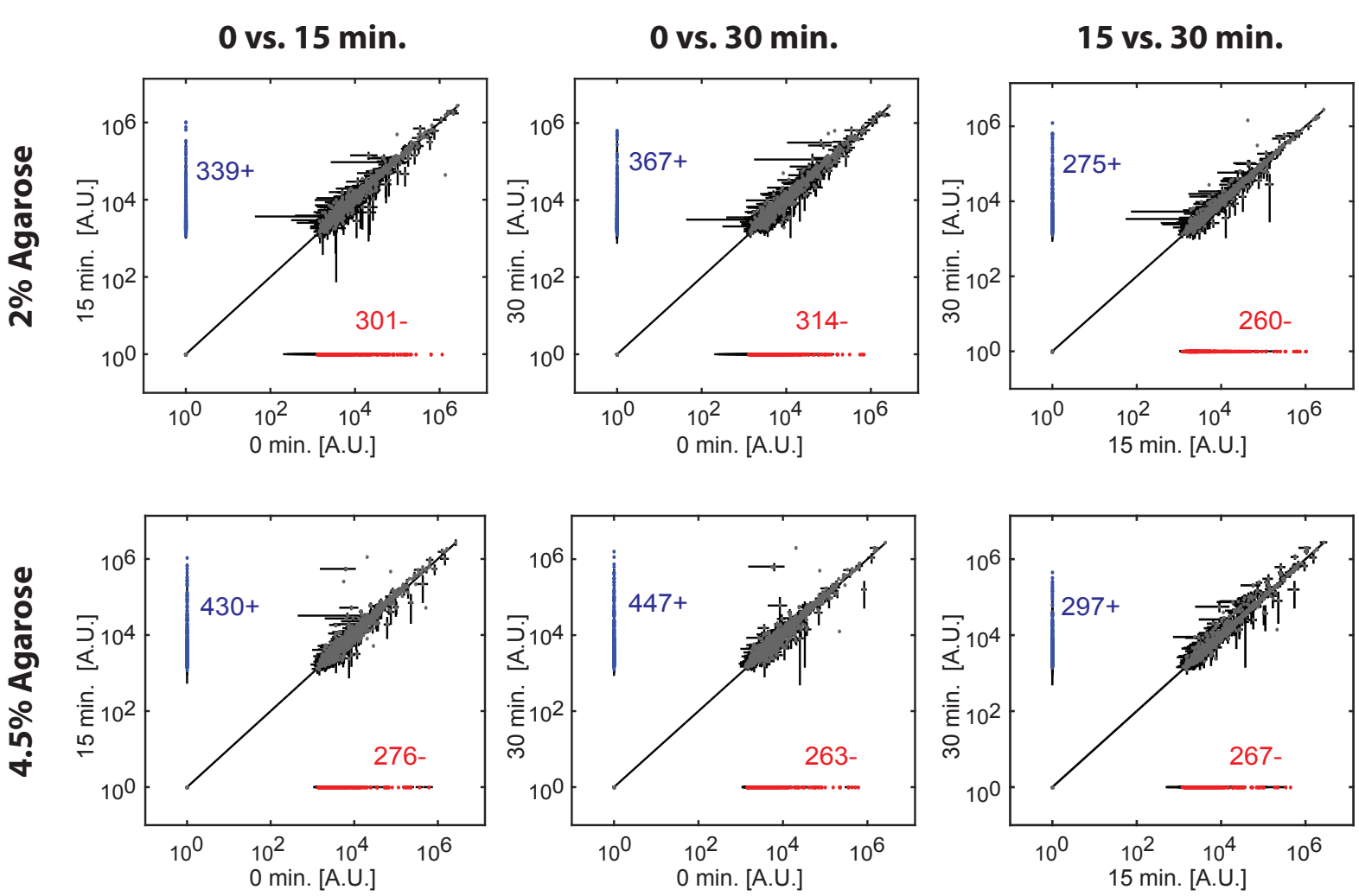
0 vs. 15 min.
0 vs. 30 min.
15 vs. 30 min.
2% Agarose
4.5% Agarose
339+
301-
367+
314-
275+
260-
430+
276-
447+
263-
297+
267-
15 min. [A.U.]
30 min. [A.U.]
0 min. [A.U.]

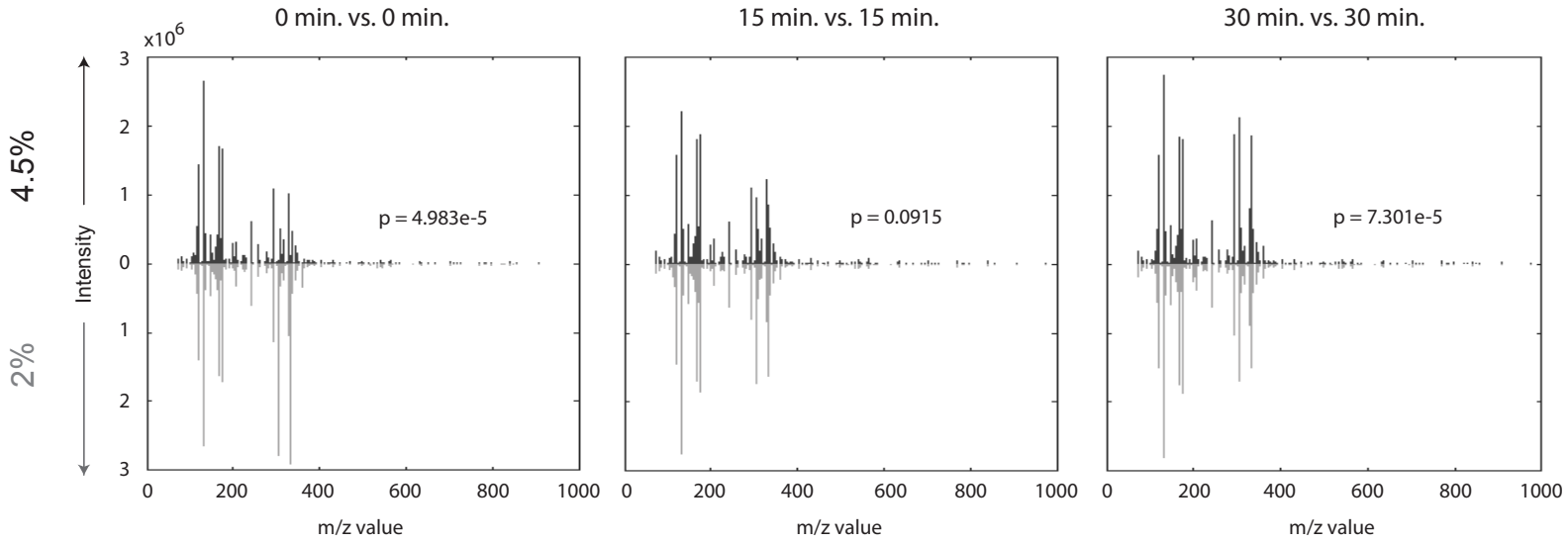
0 min. vs. 0 min.
15 min. vs. 15 min.
30 min. vs. 30 min.
4.5%
2%
Intensity
x10^6
p = 4.983e-5
p = 0.0915
p = 7.301e-5
m/z value
m/z value
m/z value

Table	Cluster	# M/Z Values	# Candidate Metabolites	# Significa Pathway
0 v 15	A1	116	342	1
	A2	126	389	8
	A3	158	711	9
	A4	517	2048	3
	A5	86	302	0
	A6	70	465	2
	A7	108	712	0
	A8	123	764	9
0 v 30	B1	83	452	1
	B2	171	797	34
	B3	135	1052	0
	B4	99	470	1
	B5	178	965	50
	B6	460	2295	10
	B7	145	645	1
	B8	154	427	1
	B9	204	989	7

Heat Map	Cluster	Cluster Description	Pathway	Mechanosensitive metabolites (KEGG ID)	Mechanosensitive metabolites (Metlin)
0 v 15	A1	↑ 2% 0 min. only	Linoleic acid metabolism	C14829;C14828;C00157	12,13 diHOME-(d4); 9,10-diHOME-(d4);PC(20:4(5Z,8Z,11Z,14Z)/22:6(4Z,7Z,10Z,13Z,16Z,19Z))
	A2	↑ 2%, ↓ 4.5%	Fatty acid/phospholipid metabolism (7)	C04230	LysoPC(18:3(6Z,9Z,12Z))
			Calcium dependent events	C04230	LysoPC(18:3(9Z,12Z,15Z))
	A3	↑ 4.5% 15 min. only	Retinol metabolism	C16677;C11061;C16680;C16679	all-trans-4-hydroxyretinoic acid; 1-O-all-trans-retinoyl-Beta-glucuronic acid; 5,6-Epoxyretinoic acid; all-trans-18-Hydroxyretinoic acid
			Vitamin A deficiency	C16677;C11061;C16680;C16679	all-trans-4-hydroxyretinoic acid; 1-O-all-trans-retinoyl-Beta-glucuronic acid; 5,6-Epoxyretinoic acid; all-trans-18-Hydroxyretinoic acid
			Adrenaline signaling (4)	C00547;C00788	Norepinephrine (noradrenaline); (-)-Epinephrine
			Platelet aggregation	C00547;C00788	Norepinephrine (noradrenaline); (-)-Epinephrine
			Alpha-linolenic acid metabolism	C16346;C16326;C16316;C04780	17-Hydroxylinolenic acid;9(S)-HOTrE; 13(S)-HOTrE; (9S,13S)-10,11-dihydro-12-oxo-15-phytoenoic acid
			Amino acid metabolism	C15975;C00671;C15979;C00233	S-(3-Methylbutanoyl)-dihydrolipoamide-E;(S)-3-Methyl-2-oxopentanoic acid; S-(2-Methylbutanoyl)-dihydrolipoamide; Ketoleucine
	A4	↑ 15 min., ↓ 0 min.	D-Glutamine/D-glutamate metabolism	C00064;C00819;C02237	L-Glutamine; D-Glutamine; (R)-(+)-2-Pyrrolidone-5-carboxylic acid
			Purine metabolism	C00064;C00362;C05239;C00262;C00020;C02348;C05516;C11821;C01367;C00294;C02350	L-Glutamine; deoxyguanosine 5\'-monophosphate (dGMP); 5-Aminoimidazole; Hypoxanthine; Adenosine monophosphate; (R)(-)-Allantoin; 5-Amino-4-imidazole carboxylate; 5-Hydroxyisourate; Adenosine 3\'-
	A5	↑ 2% 15 min. only	N/A	N/A	N/A
	A6	↑ 0 min., ↓ 15 min.	Butanoate metabolism	C01089;C05984;C02727	D(-)-Beta-hydroxy butyric acid; 2-hydroxy-butanoic acid; Nε-Acetyl-L-lysine
			Nicotinate and nicotinamide metabolism	C02295;C02930;C00922;C15986	Methylitaconate; 2-Methyleneglutarate; 2,3-Dimethylmaleate; 2,6-Dihydroxypseudooxynicotine
	A7	↑ 4.5%, ↓ 2%	N/A	N/A	N/A
	A8	↑ 4.5% 0 min. only	chondroitin sulfate degradation	C00252;C05403;C00243;C05382;C08240;C08250;C01083;C05402;C00089	Isomaltose; 3\'-Ketolactose; D-Lactose; Sedoheptulose 7-phosphate; Gentiobiose; Sophorose; Alpha,Alpha-Trehalose; Melibiose; Sucrose
			dermatan sulfate degradation	C00252;C05403;C00243;C05382;C08240;C08250;C01083;C05402;C00089	Isomaltose; 3\'-Ketolactose; D-Lactose; Sedoheptulose 7-phosphate; Gentiobiose; Sophorose; Alpha,Alpha-Trehalose; Melibiose; Sucrose
			Sugar metabolism (5)	C01083;C00243;C00208;C00089;C00252;C05731;C00185;C05400;C01235;C05402;C05403;C05382	Alpha,Alpha-Trehalose; D-Lactose; Maltose; Sucrose; Isomaltose; 3-Ketosucrose; Cellobiose; Epimelibiose; Galactinol (1-Alpha-d-galactosyl-myo-inositol); Melibiose; 3\'-Ketolactose; Sedoheptulose 7-phosphate

Heat Map	Cluster	Cluster Description	Pathway	Mechanosensitive metabolites (KEGG ID)	Mechanosensitive metabolites (Metlin)
0 v 30	B1	↑ 0 min., ↓ 30 min.	Lysine degradation	C03656;C03239;C05825;C02727;C04076	3-oxo-5S-amino-hexanoic acid; 2-Keto-6-aminocaproic acid; 2-Amino-5-oxohexanoate; Nε-Acetyl-L-lysine; L-2-Aminoadipate 6-semialdehyde
	B2	↑ 4.5% 0 min. only	chondroitin sulfate degradation	C00252;C00668;C00243;C00103;C01172;C08240;C00663;C08250;C01083;C05402;C00636;C00446;C05382;C00275;C00089	Isomaltose; Alpha-D-Glucose 6-phosphate; D-Lactose; Glucose 1-phosphate; Beta-D-Glucose 6-phosphate; Gentiobiose; Beta-D-Glucose 1-phosphate; Sophorose; Alpha,Alpha-Trehalose; Melibiose; Alpha-D-Mannose 1-phosphate; Alpha-D-Galactose 1-phD-Glucose 6-phosphateosphate; Sedoheptulose 7-phosphate; D-Mannose 6-phosphate; Sucrose
			dermatan sulfate degradation	C00252;C00668;C00243;C00103;C01172;C08240;C00663;C08250;C01083;C05402;C00636;C00446;C05382;C00275;C00089	Isomaltose; Alpha-D-Glucose 6-phosphate; D-Lactose; Glucose 1-phosphate; Beta-D-Glucose 6-phosphate; Gentiobiose; Beta-D-Glucose 1-phosphate; Sophorose; Alpha,Alpha-Trehalose; Melibiose; Alpha-D-Mannose 1-phosphate; Alpha-D-Galactose 1-phosphate; Sedoheptulose 7-phosphate; D-Mannose 6-phosphate; Sucrose
			Sugar metabolism (24)	C01083;C00243;C00103;C00018;C01094;C00668;C00085;C00208;C00446;C05382;C00105;C00089;C05400;C00092;C00252;C00668;C01172;C00663;C00185;C01083;C00208;C01097;C04006;C03546;C01177;C00085;C00275;C00636;C03267;C01094;C02888;C11544	Alpha,Alpha-Trehalose; D-Lactose; Glucose 1-phosphate; Pyridoxal Phosphate; D-Fructose 1-phosphate; Alpha-D-Glucose 6-phosphate; D-Fructose 6-phosphate; Maltose; Alpha-D-Galactose 1-phosphate; Sedoheptulose 7-phosphate; Uridine monophosphate (UMP); Sucrose; Epimelibiose; D-Glucose 6-phosphate; Isomaltose; Alpha-D-Glucose 6-phosphate; Beta-D-Glucose 6-phosphate; Beta-D-Glucose 1-phosphate; Cellobiose; Alpha,Alpha-Trehalose; Maltose; D-Tagatose 6-phosphate; 1D-myo-Inositol 3-phosphate; D-Myoinositol 4-phosphate; D-myo-Inositol-1-phosphate; D-Fructose 6-phosphate; D-Mannose 6-phosphate; Alpha-D-Mannose 1-phosphate; Beta-D-Fructose 2-phosphate; D-Fructose 1-phosphate; Sorbose 1-phosphate; 2(Alpha-D-Mannosyl)-D-glycerate;; D-Fructose 6-phosphate; Sedoheptulose 7-phosphate; D-Glucose 6-phosphate; Beta-D-Glucose 6-phosphate
			Pentose Phosphate Pathway	C00085;C05382;C00092;C01172	D-Fructose 6-phosphate; Sedoheptulose 7-phosphate; D-Glucose 6-phosphate; Beta-D-Glucose 6-phosphate;
	B3	↑ 4.5%, ↓ 2%	N/A	N/A	N/A
	B4	↑ 2%, ↓ 4.5%	Fatty acid/phospholipid metabolism	C04230;C00350	LysoPC(18:0); PE(18:4(6Z,9Z,12Z,15Z)/P-18:1(9Z))
	B5	↑ 2% 30 min. only	Fatty acid/phospholipid metabolism	C05965;C05966;C05356;C14823;C14821;C14820;C02165;C14781;C14810;C14812;C14813;C04822;C01571;C06429;C04849	12(S)-HpETE; 15(S)-HpETE; 5-Hydroperoxy-6-trans-8,11,14-cis-eicosatetraenoate (5-HPETE); 8S-HpETE; 9S-HpETE; 11R-HpETE; LTB4; (±)11,12-Ep-15(S)-HETrE; Hepoxilin B3; 12R-HpETE; 14,15-Ep-11-HETrE; 8R-HpETE; Capric acid; (4Z,7Z,10Z,13Z,16Z,19Z)-4,7,10,13,1 6,19-Docosahexaenoic acid; Hepoxilin A3
	B6	↑ 30 min., ↓ 0 min.	Alpha-linolenic acid metabolism	C16316;C16324;C16325;C16326;C04672;C16320;C00157;C16346;C16319;C01226;C04780	13(S)-HOTrE; 9,10-EOT; 10-OPDA; 9(S)-HOTrE; 12,13S-epoxy-9Z,11,15Z-octadecatrienoic acid; Colnelenic acid; PC(15:0/P-16:0); 17-Hydroxylinolenic acid; Etherolenic acid; 12-OPDA; (9S,13S)-10,11-dihydro-12-oxo-15-phytoenoic acid
			Amino acid metabolism (2)	C00064;C03406;C00669;C03465;C00233;C00791;C00248;C00407;C00078;C00399;C00487;C01252;C00547;C00624;C01259;C00123;C00209;C15767;C03415;C00791;C04281;C04282;C01877;C01682;C00624;C02647	L-Glutamine; Argininosuccinic acid; Gamma-Glu-Cys; 3-Methyl-2-oxovaleric acid; Ketoleucine; Creatinine; lipoamide; L-Isoleucine; L-Tryptophan; Ubiquinone-1; Carnitine; 4-(2-Aminophenyl)-2,4-dioxobutanoic acid; Norepinephrine (noradrenaline); N-Acetyl-L-glutamic acid; 3-Hydroxy-N6,N6,N6-trimethyl-L-lysine; L-Leucine; Oxalic acid; 4-(Glutamylamino) butanoate; N2-Succinyl-L-ornithine; Creatinine; 1-Pyrroline-4-hydroxy-2-carboxylate; 4-Oxoproline; Nopaline; N-Acetyl-L-glutamic acid; 4-Guanidinobutanal
			Retinol metabolism	C16677;C16678;C16679;C16680;C00157;C11061	all-trans-4-hydroxyretinoic acid; all-trans-4-oxoretinoic acid; all-trans-18-Hydroxyretinoic acid; 5,6-Epoxyretinoic acid; PC(15:0/P-16:0); 1-O-all-trans-retinoyl-Beta-glucuronic acid
			Vitamin A deficiency	C16677;C16678;C16679;C16680;C00157;C11061	all-trans-4-hydroxyretinoic acid; all-trans-4-oxoretinoic acid; all-trans-18-Hydroxyretinoic acid; 5,6-Epoxyretinoic acid; PC(15:0/P-16:0); 1-O-all-trans-retinoyl-Beta-glucuronic acid
			Glutathione synthesis and recycling (2)	C00064;C00669;C16673;C00407;C01879;C00078;C01259;C00123	L-Glutamine; Gamma-Glu-Cys; Isoglutamine; L-Isoleucine; Pyroglutamic acid; L-Tryptophan; 3-Hydroxy-N6,N6,N6-trimethyl-L-lysine; L-Leucine
			Metabolism of xenobiotics by cytochrom P450	C19490;C19488;C19607;C14862;C19589;C19588;C14850;C19562;C14801;C14556;C14849;C14851	trans-3,4-Dihydro-3,4-dihydroxy-7,12-dimethylbenz[a]anthracene; 7,12-Dimethylbenz[a]anthracene; trans-5,6-Dihydro-5,6-dihydroxy-7,12-dimethylbenz[a]anthracene; 2-S-Glutathionyl acetate; Aflatoxin B1 dialdehyde; Aflatoxin B1 diol; Benzo[a]pyrene-7,8-oxide; 7-Hydroxymethyl-12-methylbenz[a]anthracene sulfate; 1-Nitro-5,6-dihydroxy-dihydronaphthalene; 9-Hydroxybenzo[a]pyrene; Benzo[a]pyrene-9,10-oxide; Benzo[a]pyrene-4,5-oxide
			Protein digestion and absorption	C00064;C08262;C00407;C00078;C01468;C18319;C00123	L-Glutamine; Isovaleric acid; L-Isoleucine; L-Tryptophan; p-cresol; (±)-2-Methylbutyric acid; L-Leucine
			D-Glutamine/D-glutamate metabolism	C00064;C00819;C02237	L-Glutamine; D-Glutamine; (R)-(+)-2-Pyrrolidone-5-carboxylic acid
	B7	↑ 4.5% 30 min., ↓ 2% 0 min.	N/A	N/A	N/A
	B8	↑ 2% 0 min. only	N/A	N/A	N/A
	B9	↑ 4.5% 30 min. only	Sugar metabolism (3)	C05399;C00794;C01697;C06311;C01613;C01096;C00392;C00644	Melibiitol; D-Sorbitol; Dulcitol; Galactitol 1-phosphate; Stachyose; Sorbitol-6-phosphate; D-Mannitol; D-Mannitol 1-phosphate
			Aromatase inhibitor pathway	C08163;C08162	Letrozole; Exemestane
			Alpha-linolenic acid metabolism	C16346;C16326;C16316;C04780;C00157	17-Hydroxylinolenic acid; 9(S)-HOTrE; 13(S)-HOTrE; (9S,13S)-10,11-dihydro-12-oxo-15-phytoenoic acid; PC(14:0/20:1(11Z))
			chondroitin sulfate degradation	C00794;C05382;C01697;C02052;C01507;C01613	D-Sorbitol; Sedoheptulose 7-phosphate; Dulcitol; maltotetraose; L-Iditol; Stachyose
			dermatan sulfate degradation	C00794;C05382;C01697;C02052;C01507;C01613	D-Sorbitol; Sedoheptulose 7-phosphate; Dulcitol; maltotetraose; L-Iditol; Stachyose